Dynamic Reorganization and Correlation among Lipid Raft Components

Mónica M. Lozano,[*,†] Jennifer S. Hovis,[‡] Frank R. Moss III, and Steven G. Boxer[*]

Department of Chemistry, Stanford University, Stanford, California 94305-5012, United States

S *Supporting Information*

ABSTRACT: Lipid rafts are widely believed to be an essential organizational motif in cell membranes. However, direct evidence for interactions among lipid and/or protein components believed to be associated with rafts is quite limited owing, in part, to the small size and intrinsically dynamic interactions that lead to raft formation. Here, we exploit the single negative charge on the monosialoganglioside G_{M1}, commonly associated with rafts, to create a gradient of G_{M1} in response to an electric field applied parallel to a patterned supported lipid bilayer. The composition of this gradient is visualized by imaging mass spectrometry using a NanoSIMS. Using this analytical method, added cholesterol and sphingomyelin, both neutral and not themselves displaced by the electric field, are observed to reorganize with G_{M1}. This dynamic reorganization provides direct evidence for an attractive interaction among these raft components into some sort of cluster. At steady state we obtain an estimate for the composition of this cluster.
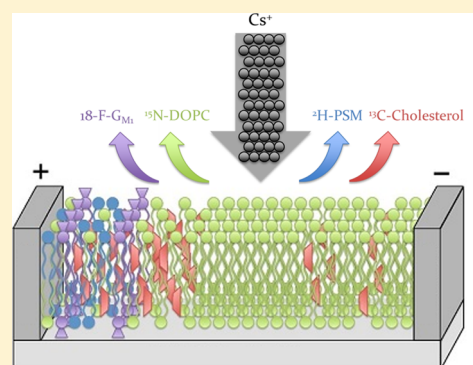
INTRODUCTION

Many biological membrane components, in particular lipids, are observed to diffuse within the plane of the membrane.[1] By itself, this fluidity suggests there can be no long-range order; however, it does not preclude the possibility of short-range order. The idea that short-range order exists, and is in fact crucial to many functions of the cell membrane, has led to the concept of lipid rafts.[2-7] In particular, nanoscale clusters of sphingolipids, cholesterol, some GPI-linked and acylated proteins, and the gangliosides are widely regarded as providing a platform for signaling, viral budding, and many other cellular functions that require the association of multiple membrane-localized components.

Raft domains are typically not directly visualized in plasma membranes due to their putative small size and dynamic nature but are inferred by specific resistance to detergent extraction, functional effects of cholesterol depletion, diffusion of dye-labeled lipids, and colocalization of certain proteins. By contrast, larger-scale lipid domains have been extensively documented in model systems such as monolayers at the air–water interface,[8] giant unilamellar vesicles (GUVs)[9] and supported lipid bilayers (SLBs),[10] along with detailed equilibrium phase diagrams.[11] While these equilibrium phase diagrams support the notion that certain components tend to interact (attractively or repulsively), the relevance of their compositions to rafts in the plasma membrane is unclear. Given the presumed dynamic nature of rafts, several groups have used measurements of lateral diffusion in cell membranes and the effect of cholesterol extraction on diffusion as a means to infer the existence, size, and dynamics of rafts.[12-15] Recent comparisons of the lipid composition of enveloped viruses and the host membranes from which they were derived provide a particularly compelling argument for the functional importance of raft compositions.[16,17] The large differences between these membrane compositions and the enrichment in the viral membranes of raft-related lipids suggest a degree of preorganization of lipid and viral protein components in the plasma membrane prior to budding.

In the following, we take a new approach to interrogating the interactions between the ganglioside G_{M1}, typically visualized by binding fluorescently labeled cholera toxin B, and cholesterol and/or sphingomyelin, components believed to be associated with rafts. We exploit the fact that G_{M1} has a single negative charge due to its sialic acid moiety, whereas cholesterol and sphingomyelin are neutral at physiological pH. Charged lipid components move in response to an electric field imposed parallel to the plane of the membrane, and when barriers to diffusion are imposed in an SLB, the competition between this electrophoretic force and random diffusion leads to a gradient of the charged component.[18,19] Other groups have used membrane electrophoresis as an analytical technique to separate charged membrane components.[20-23] The concept of the experiments reported here, illustrated schematically in Figure 1, is to selectively move G_{M1} with the electric field and then determine by imaging mass spectrometry using isotopic and atom labels (Figure 2) whether other neutral membrane components also move, i.e., whether they dynamically reorganize in concert with G_{M1}, which would demonstrate the presence of a specific, attractive interaction.
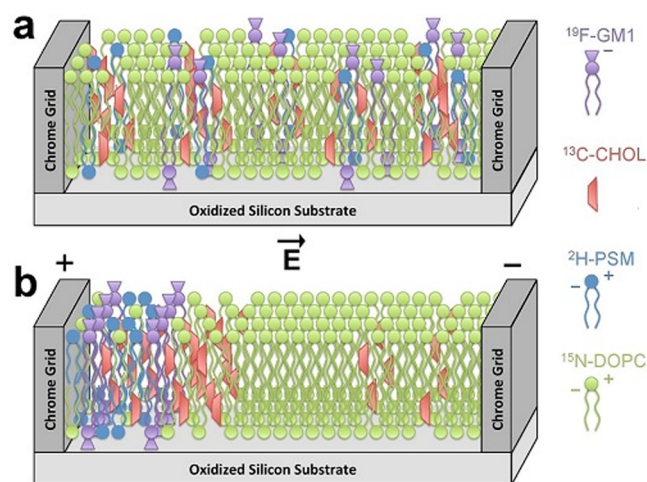
Figure 1. Reorganization of negatively charged G_{M1} may lead to reorganization of neutral membrane raft components, cholesterol, and/or sphingomyelin. Schematic of a patterned supported lipid bilayer before (a) and after (b) the application of an electric field parallel to the plane of the membrane. In this and subsequent figures, the + and − symbols above the edges are included for clarity, but note that the electrodes are far from the region being imaged.
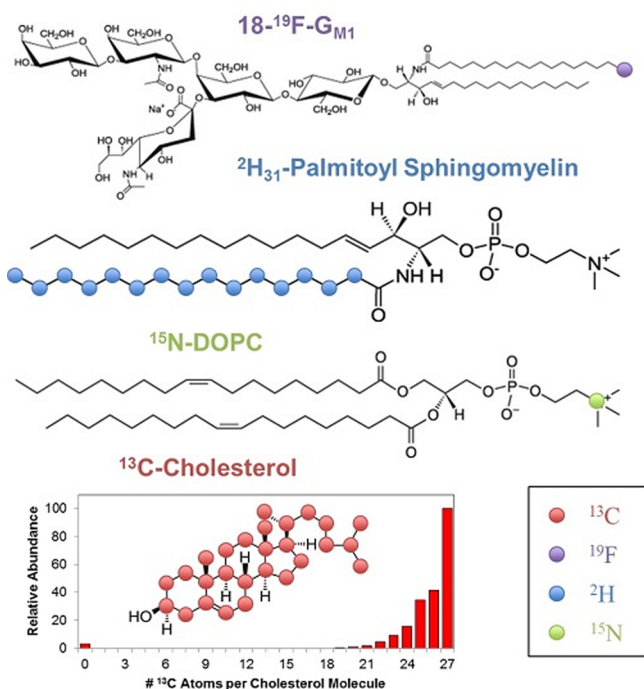

Figure 2. Structures of labeled molecules used for NanoSIMS analysis of supported lipid bilayers. The molecule-specific secondary ions are $^{12}C^{15}N^-$ for ^{15}N-DOPC, $^2H^-$ for $^2H_{31}$-sphingomyelin, F^- for 18-F-G_{M1}, and $^{12}C^{13}C^-$ for ^{13}C-cholesterol. See Figures S1 and S2 for more information on the NanoSIMS experiment. Note that G_{M1} is the only (negatively) charged component.

Previous work by our group and others has used membrane electrophoresis to study the thermodynamics of simple lipid mixtures, imaged indirectly by fluorescence, but here we extend the concept to measure specific interactions between different biologically relevant lipid species whose concentrations are analyzed directly by mass spectrometry.[24] Note that local interactions among components may be present prior to

electrophoretic reorganization, but the length scale is such that no current method can visualize this, whereas a perturbation in composition, provided by the selective movement of G_{M1}, can establish whether components tend to move together.

We emphasize the importance of using an analytical technique like imaging mass spectrometry as dye-labeled lipids can behave very differently from unlabeled lipids.[25] Furthermore, mass spectrometry can be used to obtain quantitative estimates for the mole percent of each membrane component from which information on the average stoichiometry of the interactions can be obtained.

■ RESULTS

Reorganization of G_{M1} by Membrane Electrophoresis. In order to determine whether other components also move and to avoid the potentially complicating effects of dye-labeled components, we use imaging mass spectrometry with components selectively labeled with rare stable isotopes or other atoms: G_{M1} (^{19}F), cholesterol (CHOL, ^{13}C), 1,2-dioleoyl-sn-glycero-3-phosphocholine (DOPC, ^{15}N), and palmitoyl sphingomyelin (PSM, ^2H) (Figure 2). The G_{M1} concentration gradient produced by electrophoresis (Figure 3, see also Figure
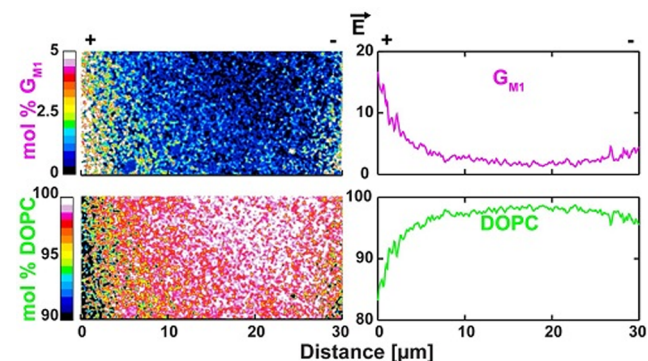

Figure 3. NanoSIMS images of the reorganization of G_{M1} in response to an electric field and the associated displacement of DOPC. NanoSIMS images and corresponding concentration profiles of a patterned supported lipid bilayer (nominal composition 99 mol % ^{15}N-DOPC and 1 mol % ^{19}F-G_{M1}) after an electric field of 7 V/cm was applied for 10 min prior to sample freezing. The chrome grids that pattern the SLB are just beyond the vertical edges of the images; signal intensities on the grid are affected by the material comprising the grid and are not shown.

S4) can be directly visualized by the unique F^- signal, and interestingly, neutral DOPC is displaced from the region where G_{M1} accumulates, thus conserving the average area per molecule. This conservation of molecular area in a fluid bilayer is expected but has never been directly visualized before.

Correlated Reorganization of G_{M1} and Other Components. NanoSIMS analysis was then used to address whether CHOL and/or PSM rearrange as G_{M1} is reorganized by an electric field. As shown in the control experiment in Figures S5 and S6, in the absence of G_{M1}, application of an electric field leaves the composition of neutral CHOL, PSM, and DOPC across the corral unchanged. By contrast, as shown in Figure 4, when G_{M1} is present the neutral CHOL does reorganize in parallel with G_{M1} upon the application of an electric field while DOPC is displaced in the opposite direction. In the quaternary mixture (Figure 5), PSM also reorganizes with G_{M1} and CHOL, while DOPC is displaced. We attempted to test the association
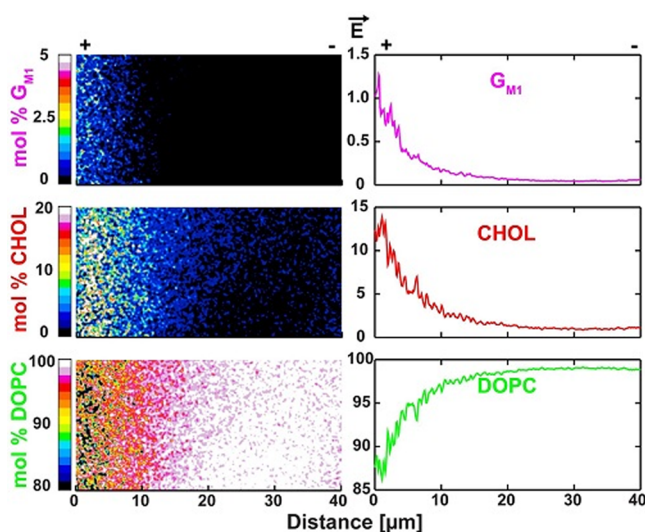
Figure 4. Correlated motion of G_{M1} and CHOL when G_{M1} is moved by an electric field. NanoSIMS images and corresponding concentration profiles of a patterned supported lipid bilayer (nominal composition 83 mol % ^{15}N-DOPC, 1 mol % ^{19}F-G_{M1}, and 16 mol % ^{13}C-cholesterol) after an electric field was applied prior to sample freezing.
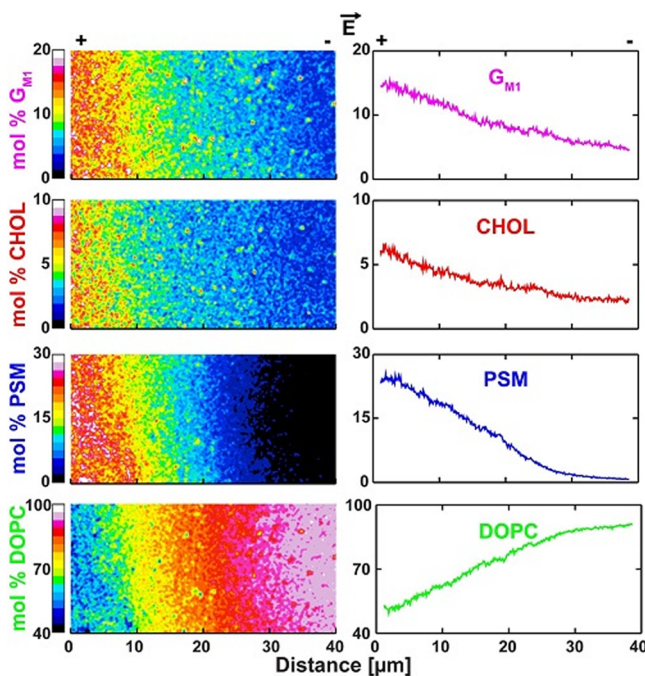

Figure 5. Correlated motion of G_{M1}, CHOL, and PSM when G_{M1} is moved by an electric field. NanoSIMS images and corresponding concentration profiles of a patterned supported lipid bilayer after an electric field was applied prior to sample freezing.

of G_{M1} with PSM in the absence of CHOL; however, small (diameter <2 μm) domains were observed for this SLB mixture prior to applying an electric field (1 mol % of G_{M1}, 8 mol % of PSM, 91 mol % of DOPC). Even though we did observe PSM move in the same direction as G_{M1} in an electric field, while background DOPC is displaced in the opposite direction within the interdomain region, consistent with the notion that G_{M1} associates with PSM, a more quantitative analysis is precluded by the observed phase separation (data not shown).

Analysis of Lipid Compositions. The overall composition of an SLB that has been reorganized within a corralled area by an applied electric field is calculated by NanoSIMS quantitative analysis.[26−29] Briefly, counts for each ion species are summed, and then the ratios $^{19}F^-/^{12}C_2^-$, $^{13}C^{12}C^-/^{12}C_2^-$, $^2H^-/^{12}C_2^-$, and $^{12}C^{15}N^-/^{12}C^{14}N^-$ are calculated. Calibration curves obtained from standard samples are then employed (see Figure S3 and Table S1) to determine the percent molar content for each component of interest. Analysis of eight corralled SLBs (see Table S2) suggests that the average (±1 std dev) overall composition of this SLB population is 9.6 ± 1.3 mol % of PSM, 7.6 ± 1.5 mol % of G_{M1}, 3.6 ± 0.9 mol % of CHOL, and 79.3 ± 2.8 mol % of DOPC. For example, the overall composition (±uncertainty) of the corralled SLB in Figure 5 is 9.2 ± 0.9 mol % of PSM, 8.8 ± 0.3 mol % of G_{M1}, 2.6 ± 1.8 mol % of CHOL, and 78.4 ± 2.4 mol % of DOPC. We note that the application of an electric field does not affect SLB composition (data not shown).

■ DISCUSSION

There are several immediate qualitative conclusions from the NanoSIMS concentration profiles: (1) in the absence of G_{M1}, the neutral CHOL, PSM, and DOPC components do not move in an electric field (Figures S4 and S5); (2) G_{M1} does move in an applied electric field toward the positive electrode and forms a concentration gradient (Figures 3 and S4); (3) when CHOL and G_{M1} are present and G_{M1} moves in an electric field, cholesterol also moves and in the same direction (Figure 4); (4) when CHOL, PSM, and G_{M1} are present and G_{M1} moves in an electric field, both CHOL and PSM move in the same direction as G_{M1} (Figure 5); and (5) neutral background DOPC is always displaced from the region where G_{M1} and other components accumulate under an applied electric field.

Taken together, these results demonstrate that both CHOL and PSM dynamically reorganize when G_{M1} reorganizes, consistent with the concept that they interact to form some sort of nanoscale cluster. We note that the shapes of the gradients in the case of the quaternary mixture (Figure 5) appear different from those in the simpler mixtures (Figures 3 and 4), and the latter are more similar to those observed for simple charged dye-labeled lipids.[18,19] The origin(s) of this difference is not yet understood; however, the purpose of this report is to establish that components interact and codiffuse and, as described in the following, to obtain an estimate for the stoichiometry of the interaction under specific conditions.

There has been considerable discussion in the literature about possible clusters formed between lipid raft components. The word cluster is used here to describe an average association number as the interactions among these components are expected to be weak and dynamic. Furthermore, we distinguish these small clusters from macroscopic phases observed in model systems and condensed complexes described for cholesterol.[9,30,31] Without information on the temperature dependence of cluster formation, we cannot determine whether the clusters of lipids that we observe represent true phases or other types of nonideal mixing. However, we emphasize that we are measuring the relative strengths of interactions between lipids, which can lead to many types of nonideal mixing behavior. Further quantitative analysis of the NanoSIMS images shown in Figure 5 allowed generation of mole fraction profiles, Y (S: PSM, G: G_{M1}, and C: CHOL), averaged perpendicular to the electric field for each component as a function of distance from the positive electrode at steady state (Figure 6). From
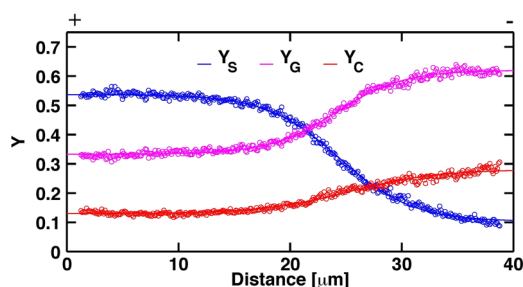
Figure 6. Mole fractions of lipid raft components at steady state derived from Figure 5. The mole fractions of G_{M1}, CHOL, and PSM are constant at $d < 20$ μm, suggesting the formation of a cluster with average composition 4:2:1 PSM/G_{M1}/CHOL. PSM appears to be the limiting reactant.

these plots, we observe that PSM, G_{M1}, and CHOL account for 23 ± 2, 15 ± 1, and 6 ± 1 mol %, respectively, at the edge closest to the cathode with the balance (54 ± 3 mol %) being filled by DOPC. The average composition in this region corresponds to the average reorganization of 4 PSM, 2 G_{M1}, and 1 CHOL molecules in response to an electric field.

The ratio of bilayer components estimated from the flat region of the mole fraction profile in Figure 6 is somewhat different from suggestions in the literature.[6,30−32] We briefly consider issues, in particular related to the possibility of G_{M1} leaflet asymmetry and possible flip−flop of components, which might affect the quantification of these values. It should be noted that the value that we calculate for the average stoichiometry of the clusters is made possible because one of the components (PSM) was the limiting reactant; if this were not the case, we would not be able to distinguish between clustered and unclustered components which would lead to an incorrect estimate in the stoichiometry calculations.

Additionally, the ratios could be different if different lipid species (e.g., POPC vs DOPC or DPPC vs PSM) were used. The average numbers of associated molecules (4:2:1, PSM/G/CHOL) estimated above from analysis of the compositional gradients for the colocalizing components are calculated from the composition of both leaflets of the SLB as the NanoSIMS cannot distinguish the composition of the upper and lower leaflets. We assume that there is no asymmetry in leaflet composition in the GUVs used to form SLBs, but G_{M1} asymmetry in supported bilayers formed from small unilamellar vesicles has previously been reported.[33−35] While lipid bilayer asymmetry would not change the qualitative finding that CHOL and PSM reorganize with G_{M1}, it would change the quantitative interpretation of the data. In the most extreme case were all G_{M1} and associated CHOL and PSM in one leaflet, one would predict phase separation based on the phase diagram for the ternary DOPC/CHOL/PSM mixture.[36] Since our bilayers appear microscopically uniform, we conclude that G_{M1} is not completely asymmetrically distributed (a more detailed discussion can be found in the SI).

The existence of dynamic subdiffraction limited clusters or complexes of CHOL and saturated phospholipids has been inferred from NMR and FRET experiments and based on thermodynamic arguments from phase diagrams.[31,37−39] In these experiments, complexes are indirectly analyzed from fatty acid chain order parameters, changes in FRET efficiency of different membrane-associated dyes, and changes in molecular areas. For monolayers of mixtures of CHOL and saturated phospholipids, the stoichiometry of complexes appears to be

approximately 1:2 CHOL/phospholipid. In monolayers, DPPC and G_{M1} form a complex with an apparent stoichiometry of 3:1 DPPC/G_{M1}.[40] Similarly, DMPC and DSPE-PEG200 form a complex in monolayers with a stoichiometry of 3:1 DMPC/DSPE-PEG2000.[41] To the best of our knowledge, these analyses have not been carried out with both G_{M1} and cholesterol in bilayers. It is not surprising that given the apparent cooperative nature of cluster formation in this quaternary mixture, the stoichiometry of complexes is different from that in simpler binary and ternary mixtures. On the other hand, analysis of the composition of detergent resistant membrane fractions suggests a more than 2:1 CHOL/PSM ratio.[42] However, this value may be skewed by effects of the detergent or by the relatively high concentration of cholesterol in the plasma membranes of most cells.[41] Although our experiments were carried out with model membranes, the existence of clusters containing CHOL and PSM in this system supports the physical possibility of nanometer-scale clusters like those proposed by the lipid raft hypothesis and provides estimates of their composition.

■ METHODS

Materials. 99% $^{13}C_6$-glucose was purchased from Cambridge Isotope Laboratories. 98% ^{15}N-choline chloride was from Sigma. *N*-Palmitoyl-d31-D-*erythro*-sphingosylphosphorylcholine ($^2H_{31}$-sphingomyelin) and 1,2-dioleoyl-*sn*-glycero-3-phosphate (sodium salt) (DOPA) were from Avanti Polar Lipids. All other reagents were from Fisher and were used as supplied.

Biosynthesis and Purification of ^{13}C-Cholesterol. *Saccharomyces cerevisiae* strain RH6829, which produces cholesterol as its primary sterol, was obtained from Prof. Riezman (University of Geneva).[43] Cholesterol was metabolically labeled with $^{13}C_6$-glucose and purified with HPLC according to the procedure of Shivapurkar et al.[44] Briefly, RH6829 yeast were grown in minimal media with 1.5% u-$^{13}C_6$ (99 atom %) glucose as the sole carbon source. After being shaken at 230 rpm at 30 °C for 2 days, cells were subjected to alkaline methanolysis. Lipids were extracted with petroleum ether, and cholesterol was purified from the lipid extract with HPLC. The extent of labeling and purity was assessed with GC−MS (see inset, Figure 2). Approximately 5 mg of labeled cholesterol per liter of media was obtained under these conditions.

Synthesis of ^{15}N-DOPC. ^{15}N-DOPC was synthesized by esterifying DOPA with ^{15}N-choline as previously described.[26,45] Briefly, 515 mg of ^{15}N-choline chloride, 264 mg of DOPA, and 20 mL of anhydrous pyridine were added to a round-bottom flask with a stir bar. A 3.47 mL portion of trichloroacetonitrile was slowly added to the flask, and the mixture was stirred at 60 °C overnight. The solution was cooled, filtered, and concentrated via rotary evaporation. The resulting brown residue was dissolved in 40 mL of CH_3OH/$CHCl_3$(1:1) and again concentrated via rotary evaporation. The product was purified via column chromatography on IWT TMD-8 ion-exchange resin (50% tetrahydrofuran in water), followed by column chromatography on silica gel ($CHCl_3$/CH_3OH/H_2O 65:25:4) and column chromatography on octadecyl-functionalized silica gel ($CHCl_3$/CH_3OH 5:95), yielding the pure phosphatidylcholine (92.9 mg, 32.2% yield) as a white solid.

Synthesis of 18-F-G_{M1}. Monofluorinated G_{M1} (18-F-G_{M1}) was synthesized by coupling lyso-G_{M1} with the corresponding fluorinated stearic acid.[26] Briefly, lyso-G_{M1} was obtained by alkaline hydrolysis of native G_{M1} and then treated with the *N*-hydroxysuccinimide (NHS) ester of the 18-monofluorinated stearic acid in diisopropylethyl amine to yield the fluorinated G_{M1}. The product was purified by flash column chromatography ($CHCl_3$/CH_3OH/H_2O, 60:40:5). Note that it was shown in previous work that the 18-F-G_{M1} behaves identically as native G_{M1}.[26]

SLB Formation and Electrophoresis. Patterned supported lipid bilayers were formed from giant unilamellar vesicles (GUVs, typically

tens of microns in diameter) that were deposited on chrome-patterned (grid dimensions between 35 μm × 35 and 50 μm × 50 μm), oxidized silicon substrates by allowing them to rupture spontaneously and fill in the corralled regions created by the chrome grids. GUVs were electroformed by spreading 10 μL of a lipid mixture (1:99 G_{M1}/DOPC, 1:16:83 G_{M1}/cholesterol/DOPC, 16:8:76 cholesterol/sphingomyelin/DOPC, or 1:16:8:75 G_{M1}/cholesterol/sphingomyelin:DOPC) in chloroform (5 mM total lipid concentration) on the platinum wires of a homemade electroformation chamber. GUVs were formed by applying a sinusoidal current (3 V peak-to-peak at 10 Hz) at 55 °C for 2 h. A low concentration of a negatively charged, fluorescently labeled lipid (i.e., 0.05 mol % TR-DHPE) was added to the lipid mixture to allow visualization of the supported lipid bilayers during the electrophoresis experiment. The negative charge on the fluorescent lipid allowed real-time visualization of lipid reorganization in response to an electric field (i.e., visualize the emergence of a fluorescence gradient). Fluorescence imaging was performed using a Nikon Eclipse 80i epifluorescence microscope equipped with an Andor Clara camera.

The membrane electrophoresis cell consisted of two 0.5 mm platinum wire electrodes 6 cm apart and a glass coverslip arranged to form a bridge between the electrodes. Electrical connection was achieved through water (Milli-Q, resistivity = 18.2 MΩ cm) contact. The cell was rinsed thoroughly to remove residual salt deposits. An electric field of 7 V/cm for 10 min was applied with a standard power supply (current <0.001 mA which produced a negligible amount of resistive heating). Note that substantially higher fields can be applied to SLBs on glass than on the Si substrates used for NanoSIMS measurements. All experiments were performed at room temperature.

Freeze-Drying Samples. Because NanoSIMS analysis takes place in an ultrahigh vacuum, lipid bilayer samples must be dehydrated. To preserve the lateral organization of lipid bilayers formed in an aqueous environment, techniques from electron microscopy were applied.[45] Briefly, supported lipid bilayer samples on the NanoSIMS supports were carefully removed from their aqueous environment with tweezers and flash-frozen by plunging quickly into a chamber filled with liquid N_2. The frozen samples were then subjected to reduced pressures (70−80 μbar) generated by an oil-free scroll pump equipped with a liquid N_2 trap for at least 12 h to sublime vitreous ice. The final product was a dehydrated lipid bilayer shown to have identical features from its original hydrated state.[26,28] Note that the time between the end of application of the electric field and flash freezing is only a few seconds during which only limited lateral diffusion of membrane components can occur.

NanoSIMS imaging. SIMS imaging was performed using the NanoSIMS 50L instrument at Stanford University, and the experiment is illustrated schematically in Figure S1. The measurements were made in Images analysis mode using a ∼ 2 pA $^{133}Cs^+$ primary ion beam (with an approximately 8% conversion based on the detection of $^{28}Si^-$ secondary ions from a Si wafer) focused to a ∼100 nm diameter spot and rastered over sample areas that were between 35 μm × 35 and 50 μm × 50 μm. The images consisted of 10 scans (long enough to remove all lipid material from the surface) of 512 × 512 pixels with a dwell time of 1 ms/pixel. Secondary ion intensities for $^2H^-$, $^{19}F^-$, $^{12}C^{12}C^-$, $^{12}C^{13}C^-$, $^{12}C^{14}N^-$, and $^{12}C^{15}N^-$ were collected simultaneously in Multicollection mode. Mass resolving powers of ∼6600 were used to separate isobaric interferences $^{12}C^{15}N^-$ from $^{13}C^{14}N^-$ at mass 27 (Figure S2). Samples were also simultaneously imaged using secondary electrons.

Data Analysis. Data analysis was performed using the open source software Open MIMS, which is an ImageJ (v. 1.44o, National Institutes of Health) plugin. For qualitative (i.e., visualization) purposes only, each ratio image was smoothed (binned) by replacing the pixel value with the average of its 3 × 3 neighboring pixels for noise reduction while the original image was used for all quantitative analyses. Quantitative compositional analysis was obtained through the use of calibration curves from standard samples (see Figure S3 and Table S1). Calibration curves were obtained by analyzing standard samples prepared from each molecule of interest (i.e., ^{13}C-cholesterol, ^2H-sphingomyolin, and ^{19}F-G_{M1}) at specific molar percentages with

the balance molar percentage consisting of ^{15}N-DOPC. A calibration curve for ^{15}N-DOPC was obtained as previously described (Figure S3).[26]

■ ASSOCIATED CONTENT

⑤ Supporting Information

The Supporting Information is available free of charge on the ACS Publications website at DOI: 10.1021/jacs.6b05540.

> Schematic of the NanoSIMS experiment (Figure S1); HMR spectra (Figure S2) and calibration curves and parameters (Figures S3 and Table S1); preliminary electric field experiment results (Figure S4); CHOL/PSM/DOPC NanoSIMS images and profiles (Figures S5−S6); composition and stoichiometry calculations (Table S2−S3) (PDF)

■ AUTHOR INFORMATION

Corresponding Authors
*mmlozano@gmail.com
*sboxer@stanford.edu

Present Addresses
†Nanotech Biomachines, Inc., Berkeley, CA 94710.
‡Genia, Mountain View, CA 94043.

Notes
The authors declare no competing financial interest.

■ ACKNOWLEDGMENTS

■ REFERENCES

(1) Singer, S. J.; Nicolson, G. L. *Science* **1972**, *175*, 720−731.
(2) Jain, M. K.; White, H. B., III *Adv. Lipid Res.* **1977**, *15*, 1−60.
(3) Thompson, T. E.; Tillack, T. W. *Annu. Rev. Biophys. Biophys. Chem.* **1985**, *14*, 361−386.
(4) Brown, D. A.; Rose, J. K. *Cell* **1992**, *68*, 533−544.
(5) Simons, K.; Ikonen, E. *Nature* **1997**, *387*, 569−572.
(6) Edidin, M. *Annu. Rev. Biophys. Biomol. Struct.* **2003**, *32*, 257−283.
(7) Jacobson, K.; Mouritsen, O. G.; Anderson, R. G. *Nat. Cell Biol.* **2007**, *9*, 7−14.
(8) McConnell, H. M. *Annu. Rev. Phys. Chem.* **1991**, *42*, 171−195.
(9) Veatch, S. L.; Keller, S. L. *Biophys. J.* **2003**, *85*, 3074−3083.
(10) Crane, J. M.; Tamm, L. K. *Biophys. J.* **2004**, *86*, 2965−2979.
(11) Feigenson, G. W. *Nat. Chem. Biol.* **2006**, *2*, 560−563.
(12) Honigmann, A.; Mueller, V.; Hell, S. W.; Eggeling, C. *Faraday Discuss.* **2013**, *161*, 77−89 and discussion 113−50.
(13) Eggeling, C.; Ringemann, C.; Medda, R.; Schwarzmann, G.; Sandhoff, K.; Polyakova, S.; Belov, V. N.; Hein, B.; von Middendorff, C.; Schonle, A.; Hell, S. W. *Nature* **2009**, *457*, 1159−1162.

(14) Kusumi, A.; Suzuki, K. *Biochim. Biophys. Acta, Mol. Cell Res.* **2005**, *1746*, 234−251.

(15) Kusumi, A.; Tsunoyama, T. A.; Hirosawa, K. M.; Kasai, R. S.; Fujiwara, T. K. *Nat. Chem. Biol.* **2014**, *10*, 524−532.

(16) Brugger, B.; Glass, B.; Haberkant, P.; Leibrecht, I.; Wieland, F. T.; Krausslich, H. G. *Proc. Natl. Acad. Sci. U. S. A.* **2006**, *103*, 2641−2646.

(17) Gerl, M. J.; Sampaio, J. L.; Urban, S.; Kalvodova, L.; Verbavatz, J. M.; Binnington, B.; Lindemann, D.; Lingwood, C. A.; Shevchenko, A.; Schroeder, C.; Simons, K. *J. Cell Biol.* **2012**, *196*, 213−221.

(18) Groves, J. T.; Boxer, S. G. *Biophys. J.* **1995**, *69*, 1972−1975.

(19) Groves, J. T.; Boxer, S. G. *Acc. Chem. Res.* **2002**, *35*, 149−157.

(20) Poyton, P. F.; Cremer, P. F. *Anal. Chem.* **2013**, *85*, 10803−10811.

(21) Monson, C. F.; Pace, H. P.; Liu, C.; Cremer, P. S. *Anal. Chem.* **2011**, *83*, 2090−2096.

(22) Daniel, S.; Diaz, A. J.; Martinez, K. M.; Bench, B. J.; Albertorio, F.; Cremer, P. S. *J. Am. Chem. Soc.* **2007**, *129*, 8072−8073.

(23) Pace, H. P.; Sherrod, S. D.; Monson, C. F.; Russell, D. H.; Cremer, P. S. *Anal. Chem.* **2013**, *85*, 6047.

(24) Roth, J. S.; Zhang, Y.; Bao, P.; Cheetham, M. R.; Han, X.; Evans, S. D. *Appl. Phys. Lett.* **2015**, *106*, 183703.

(25) Hughes, L. D.; Rawle, R. J.; Boxer, S. G. *PLoS One* **2014**, *9*, e87649.

(26) Lozano, M. M.; Liu, Z.; Sunnick, E.; Janshoff, A.; Kumar, K.; Boxer, S. G. *J. Am. Chem. Soc.* **2013**, *135*, 5620−5630.

(27) Kraft, M. L.; Fishel, S. F.; Marxer, C. G.; Weber, P. K.; Hutcheon, I. D.; Boxer, S. G. *Appl. Surf. Sci.* **2006**, *252*, 6950−6956.

(28) Kraft, M. L.; Weber, P. K.; Longo, M. L.; Hutcheon, I. D.; Boxer, S. G. *Science* **2006**, *313*, 1948−1951.

(29) Galli Marxer, C.; Kraft, M. L.; Weber, P. K.; Hutcheon, I. D.; Boxer, S. G. *Biophys. J.* **2005**, *88*, 2965−2975.

(30) McConnell, H. M.; Radhakrishnan, A. *Biochim. Biophys. Acta, Biomembr.* **2003**, *1610*, 159−173.

(31) Radhakrishnan, A.; Li, X. M.; Brown, R. E.; McConnell, H. M. *Biochim. Biophys. Acta, Biomembr.* **2001**, *1511*, 1−6.

(32) Pike, L. J. *J. Lipid Res.* **2003**, *44*, 655−667.

(33) Ajo-Franklin, C. M.; Yoshina-Ishii, C.; Boxer, S. G. *Langmuir* **2005**, *21*, 4976−4983.

(34) Shreve, A. P.; Howland, M. C.; Sapuri-Butti, A. R.; Allen, T. W.; Parikh, A. N. *Langmuir* **2008**, *24*, 13250−13253.

(35) Carton, I.; Malinina, L.; Richter, R. P. *Biophys. J.* **2010**, *99*, 2947−2956.

(36) Veatch, S. L.; Keller, S. L. *Biophys. J.* **2003**, *85*, 3074−3083.

(37) Radhakrishnan, A.; Anderson, T. G.; McConnell, H. M. *Proc. Natl. Acad. Sci. U. S. A.* **2000**, *97*, 12422−12427.

(38) Lee, K. Y.; Klingler, J. F.; McConnell, H. M. *Science* **1994**, *263*, 655−658.

(39) Veatch, S. L.; Polozov, I. V.; Gawrisch, K.; Keller, S. L. *Biophys. J.* **2004**, *86*, 2910−2922.

(40) Frey, S. L.; Chi, E. Y.; Arratia, C.; Majewski, J.; Kjaer, K.; Lee, K. Y. C. *Biophys. J.* **2008**, *94*, 3047−3064.

(41) Lozano, M. M.; Longo, M. L. *Soft Matter* **2009**, *5*, 1822−1834.

(42) Otahal, P.; Angelisova, P.; Hrdinka, M.; Brdicka, T.; Novak, P.; Drbal, K.; Horejsi, V. *J. Immunol.* **2010**, *184*, 3689−3696.

(43) Souza, C. M.; Schwabe, T. M.; Pichler, H.; Ploier, B.; Leitner, E.; Guan, X. L.; Wenk, M. R.; Riezman, I.; Riezman, H. *Metab. Eng.* **2011**, *13*, 555−569.

(44) Shivapurkar, R.; Souza, C. M.; Jeannerat, D.; Riezman, H. *J. Lipid Res.* **2011**, *52*, 1062−1065.

(45) Boxer, S. G.; Kraft, M. L.; Weber, P. K. *Annu. Rev. Biophys.* **2009**, *38*, 53−74.